Thermoelectric and thermospin transport in a ballistic junction of graphene

M. Inglot,[1] V. K. Dugaev,[2,3] and J. Barnaś[4,5]

[1]*Research and Development Centre for Photovoltaics, ML System S.A., ul. Warszawska 50D, 35-230 Rzeszów, Poland*
[2]*Department of Physics, Rzeszów University of Technology, al. Powstańców Warszawy 6, 35-959 Rzeszów, Poland*
[3]*Departamento de Física and CeFEMA, Instituto Superior Técnico, Universidade de Lisboa, Avenida Rovisco Pais, 001-1049 Lisboa, Portugal*
[4]*Faculty of Physics, Adam Mickiewicz University, ul. Umultowska 85, 61-614 Poznań, Poland*
[5]*The Nano-Bio-Medical Centre, Umultowska 85, 61-614 Poznań, Poland*

(Received 16 April 2015; revised manuscript received 27 July 2015; published 17 August 2015)

We consider theoretically a wide graphene ribbon that is attached on both ends to electronic reservoirs, which generally have different temperatures. The graphene ribbon is assumed to be deposited on a substrate that leads to a spin-orbit coupling of the Rashba type. We calculate the thermally induced charge current in the ballistic transport regime as well as the thermoelectric voltage (Seebeck effect). Apart from this, we also consider thermally induced spin current and spin polarization of the graphene ribbon. The spin currents are shown to have generally two components; one parallel to the temperature gradient and the other perpendicular to this gradient. The latter corresponds to the spin current due to the spin Nernst effect. Additionally, we also consider the heat current between the reservoirs due to transfer of electrons.

DOI: 10.1103/PhysRevB.92.085418 PACS number(s): 72.25.Fe, 78.67.Wj, 81.05.ue, 85.75.−d

I. INTRODUCTION

Low-energy electronic states in graphene—a two-dimensional (2D) hexagonal lattice of carbon atoms—are usually described by the relativistic Dirac model [1]. The unique transport properties of graphene, especially the high electron velocity and the tendency to avoid electron scattering due to the Klein effect, make graphene an excellent material for future applications in nanoelectronics [2,3]. These properties also facilitate practical realization of ballistic junctions based on graphene [4,5]. Indeed, such junctions have been extensively studied in recent years [6–8]. It has been shown, for instance, that junctions of two graphene parts corresponding to different Rashba coupling parameters exhibit interesting transport properties [9]. When the graphene is additionally magnetized, e.g., due to coupling to an insulating magnetic substrate, a large anisotropic magnetoresistance effect can then be observed [10].

Remarkably less theoretical and experimental work has been done up to now on the thermoelectric properties of graphene, though interest in these properties has grown recently [11–22]. Theoretical works were focused mainly on the diffusion transport regime in graphene with impurities and other structural defects. It has been shown, for instance, that under certain conditions the Wiedemann-Franz law can be violated in graphene [23]. Moreover, resonant scattering from impurities with short-range potential may lead to an enhanced Seebeck coefficient, when the chemical potential is in the neighborhood of the resonances [24–27]. Of particular interest are currently the thermoelectric properties of graphene nanoribbons, which may exhibit an enhanced thermoelectric efficiency [28–34]. This efficiency may additionally be enhanced by certain structural defects, such as antidots, for instance [14]. In addition, there is currently great interest in spin-related thermoelectric phenomena in nanoscale systems, including also graphene nanostructures. It has been shown, among others, that graphene nanoribbons with zigzag edges can exhibit not only conventional but also spin thermoelectricity [14]. The latter corresponds to a spin voltage generated by a temperature gradient. Various physical phenomena associated with thermally induced spin and heat currents are also of current interest [35,36].

One may have observed recently the increased interest in the ballistic transport regime [37,38]. This is due to the possibility of a long mean free path ℓ in 2D electron gas [38], where $\ell \simeq 3\ \mu$m has already been reached [39], and in graphene nanoribbons, where $\ell > 10\ \mu$m has been reported [40]. The main objective of this paper is a theoretical description of thermoelectric and thermospin transport properties of ballistic graphene junctions. We calculate the thermoelectrically induced charge and spin currents in a graphene ribbon of length L, which is attached to two electronic reservoirs. The ribbon length is assumed to be smaller than the corresponding electron mean free path ℓ. The main focus of the paper is on the spin effects due to spin-orbit interaction in graphene. Since the intrinsic spin-orbit coupling in graphene is very small, it is neglected here. In turn, the Rashba spin-orbit coupling related to the influence of a substrate can be relatively strong, and therefore it is included in our considerations. We show that a temperature gradient in the presence of Rashba spin-orbit coupling can generate in graphene not only a spin current flowing perpendicularly to the temperature gradient (spin Nernst effect) but also a spin density (spin polarization). It is worth noting that a similar problem was considered in a recent paper by Gusynin *et al.* [41], where the spin Nernst effect in 2D materials with a buckled hexagonal lattice (like silicene for instance) was analyzed theoretically. However, the model considered in this paper was different, as the authors included the intrinsic spin-orbit interaction and neglected spin-orbit coupling of the Rashba type. It is worth noting that the corresponding spin current can be also generated by an external electric field (spin Hall effect) [42,43]. Similarly, spin polarization can be induced by the electric field as well [41,44].

In Sec. II we describe the theoretical model. Numerical results on the thermally induced charge and heat currents are

presented and discussed in Sec. III. In turn, thermally induced spin current and spin polarization of graphene is considered in Sec. IV. A summary and final conclusions are given in Sec. V.

II. MODEL

We assume the relativistic Hamiltonian for electrons in graphene with Rashba spin-orbit coupling,

$$H_{\mathbf{k}} = \hbar v_F \boldsymbol{\tau} \cdot \mathbf{k} + \lambda(\sigma_x \tau_y - \sigma_y \tau_x), \tag{1}$$

where v_F is the electron velocity in graphene, $\mathbf{k} = (k_x, k_y)$ is a 2D wave vector, $\lambda = \alpha/2$, and α is the Rashba spin-orbit coupling parameter, while $\boldsymbol{\tau}$ and $\boldsymbol{\sigma}$ are the vectors of Pauli matrices defined in the sublattice and spin spaces, respectively. Hamiltonian (1) describes low-energy electron states in the vicinity of the Dirac point K of the corresponding Brillouin zone. The Hamiltonian for the second nonequivalent Dirac point, K', can be obtained from Eq. (1) by reversing the sign of the wave-vector component k_x.

The electronic band structure described by Hamiltonian (1) consists of four energy bands,

$$\varepsilon_{\mathbf{k}n} = \pm\lambda \pm \left(\hbar^2 v_F^2 k^2 + \lambda^2\right)^{1/2}, \tag{2}$$

where $n = 1$ to 4 is the band index, with $n = 1$ ($n = 4$) corresponding to the band of the lowest (highest) energy. Each of the bands is parabolic at small wave vectors, $k \ll \lambda/\hbar v_F$, and has an almost-linear dispersion for $k \gg \lambda/\hbar v_F$. The valence band corresponding to $n = 2$ and the conduction band corresponding to $n = 3$ touch at $k = 0$, while two others ($n = 1,4$) are separated by an energy gap of width equal to 2α.

We assume that the x axis is along the graphene ribbon of length L, as shown schematically in Fig. 1. The ribbon is wide enough to neglect size quantization. In turn, the length L is smaller than the mean free path ℓ, $L \ll \ell$, so electronic transport can be considered fully ballistic. For simplicity, we neglect any scattering of electrons inside the ribbon. Additionally, we assume that the graphene ribbon is in contact at the ends with two 2D electronic reservoirs, which generally have different temperatures, T_1 and T_2, as indicated in Fig. 1. Electrons in these reservoirs are described by the

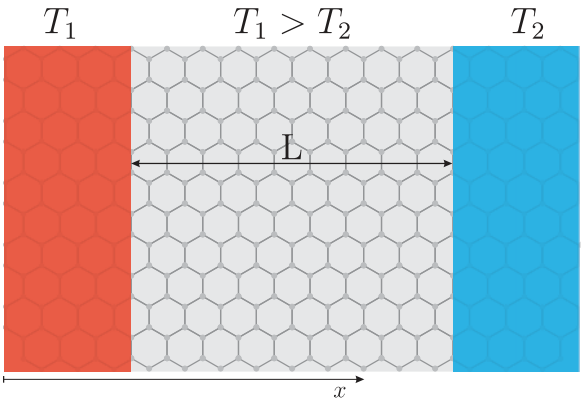

FIG. 1. (Color online) Schematic of a ballistic junction consisting of a graphene ribbon of length L and two 2D electronic reservoirs. The reservoirs have generally different temperatures, as indicated.

corresponding equilibrium Fermi-Dirac distribution functions,

$$f_{1,2}(\varepsilon_{\mathbf{k}n}) = [\exp((\varepsilon_{\mathbf{k}n} - \mu_{1,2})/k_B T_{1,2}) + 1]^{-1}, \tag{3}$$

where μ_1 and μ_2 are the chemical potentials. Though we are focused mainly on thermal effects, we assume that μ_1 and μ_2 can be different in a general situation. Thus, the electron system in the ballistic regime can be described by the distribution functions $f_1^>(\varepsilon_{\mathbf{k}n})$ and $f_2^<(\varepsilon_{\mathbf{k}n})$ for electrons moving from left to right and from right to left, respectively. In the following we use these distribution functions to calculate transport and thermoelectric properties of the graphene ribbon, assuming a purely ballistic regime.

III. THERMALLY INDUCED CHARGE AND HEAT CURRENTS

Assume equal chemical potentials in the two electronic reservoirs, $\mu_1 = \mu_2 = \mu$, and different temperatures, $T_1 = T + \Delta T > T_2 = T$. The former condition is relaxed only when necessary. Below we calculate the charge current due to the temperature difference (gradient) and, also, the corresponding electronic contribution to the heat current.

A. Charge current

The charge current in the ballistic transport regime, flowing along the axis x due to the difference $\Delta T = T_1 - T_2 > 0$ in the reservoir temperatures, can be calculated with the formula

$$j = e \sum_n {\sum_{\mathbf{k}}}' \langle \mathbf{k}n|\hat{v}_x|\mathbf{k}n\rangle [f_1^>(\varepsilon_{\mathbf{k}n}) - f_2^<(\varepsilon_{\mathbf{k}n})], \tag{4}$$

where e is the electron charge, $\hat{v}_x = v_F \tau_x$ is the electron velocity operator, and the summation over the wave vector $\mathbf{k}$ is restricted to the angles for which the x component of the electron velocity, $v_{xn} = \langle \mathbf{k}n|\hat{v}_x|\mathbf{k}n\rangle$, is positive.

For definiteness, we assume that the chemical potential of electrons is positive, $\mu > 0$. It is clear that due to the electron-hole symmetry, the results for $\mu < 0$ can differ only in sign from those for $\mu > 0$. This is because the electron velocity v_{xn} is positive for $k_x > 0$ in energy bands with $\varepsilon_{\mathbf{k}n} > 0$ and negative for bands with $\varepsilon_{\mathbf{k}n} < 0$.

The thermoelectric current calculated as a function of ΔT is presented in Fig. 2(a) for different values of the Rashba coupling constant α (including $\alpha = 0$), while the corresponding dependence on the chemical potential μ is shown in Fig. 2(b). From Fig. 2(a) it follows that the magnitude of current increases nonlinearly with ΔT when $\Delta T/T \gg 1$. In the low-ΔT limit, in turn, this increase is rather linear in ΔT.

Variation of the thermoelectric current with the chemical potential μ is shown in Fig. 2(b) for a few values of the Rashba parameter. Independently of the Rashba coupling strength, the current vanishes for $\mu = 0$, i.e., when the Fermi level is at the particle-hole symmetry point. The particle and hole currents then compensate each other. Consider now the dependence on α and let us start with the case of no Rashba coupling, $\alpha = 0$. Since the particle current is higher (for positive μ) due to the linear variation of the density of states with increasing energy, the absolute magnitude of the current increases with increasing μ. When $\mu \lesssim kT_1, kT_2$, the hole current is rather low

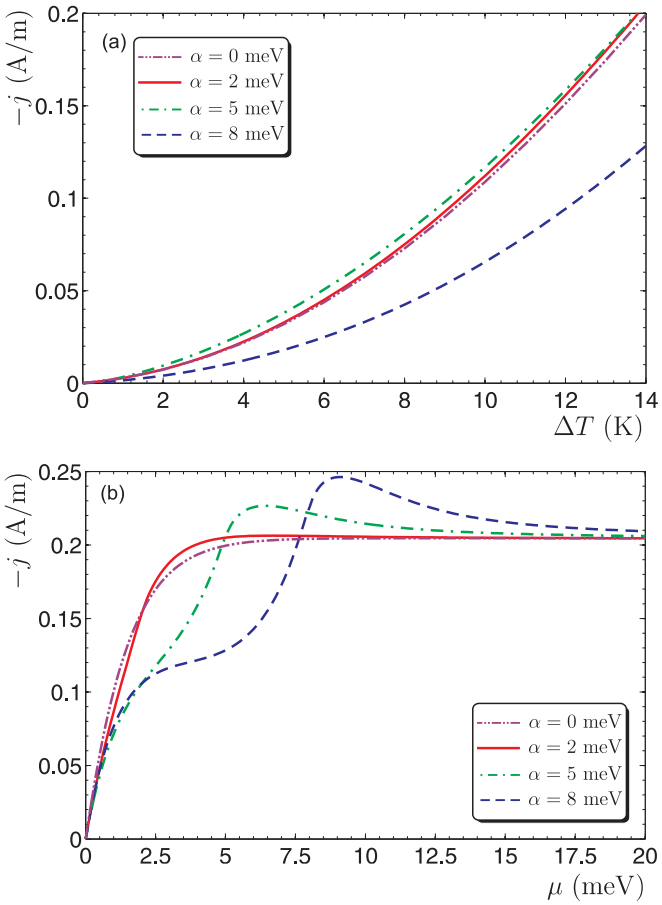

FIG. 2. (Color online) Thermoelectric current in the ballistic regime as a function of ΔT (a) and chemical potential μ (b) for indicated values of the Rashba coupling parameter α, $T = 1$ K, and for $\mu = 5$ meV (a) and $\Delta T = 14$ K (b).

due to small contributions from the valance and conduction bands (the former decreases with increasing μ). As a result, the magnitude of current then increases with increasing μ. When $\mu \gg kT_1, kT_2$, then only conduction bands (degenerate) contribute to the current and the current saturates at a constant value which is independent of μ. Though the particle and whole currents both increase with increasing μ, they do not compensate each other and their sum remains constant.

When $0 \leqslant \alpha \lesssim kT_1, kT_2$, then the behavior of the current with increasing μ is similar to that for $\alpha = 0$ [see the curves for $\alpha = 0$ and $\alpha = 2$ meV in Fig. 2(b)]. If, however, $\alpha \gg kT_1, kT_2$, then a plateau in the current appears for $kT_1, kT_2 \lesssim \mu \lesssim \alpha$. When the chemical potential increases further, the current increases when the bottom of the conduction sub-band at $\mu = \alpha$ is approached. When μ exceeds α, then a maximum appears in the current, which is due to the enhanced density of states at the bottom of the sub-band. This is because the dispersion relation is then parabolic rather than linear. The position of this peak roughly corresponds to the band edge of the second conduction band, which appears at $\varepsilon = \alpha$. When μ increases further, the current decreases, approaching the value for graphene with zero Rashba coupling. This is because the influence of Rashba coupling on the electronic bands then becomes diminished and the dispersion relations tend to linear ones.

In the linear response regime one may obtain some analytical results. Indeed, in the limit of a small temperature difference, $\Delta T/T \ll 1$, one can use

$$f_1^{>}(\varepsilon_{\mathbf{k}n}) - f_2^{<}(\varepsilon_{\mathbf{k}n}) \simeq -\frac{\Delta T}{T}(\varepsilon_{\mathbf{k}n} - \mu)\frac{\partial f}{\partial \varepsilon_{\mathbf{k}n}}. \tag{5}$$

Using Eqs. (3) and (5) we obtain

$$\begin{aligned} j &= \frac{e\,\Delta T}{2\pi T}\sum_n \int_0^\infty d\varepsilon \int_{-\pi/2}^{\pi/2} d\phi \nu_n(\varepsilon)\nu_n(\varepsilon)\cos\phi \\ &\quad \times(\varepsilon - \mu)\left(-\frac{\partial f}{\partial \varepsilon}\right) \\ &= \frac{e\Delta T}{\pi T}\sum_n \int_0^\infty d\varepsilon \nu_n(\varepsilon)\nu_n(\varepsilon)(\varepsilon - \mu)\left(-\frac{\partial f}{\partial \varepsilon}\right), \end{aligned} \tag{6}$$

where $\nu_n(\varepsilon)$ and $v_n(\varepsilon)$ are the density of states and electron velocity in the nth band, respectively. At rather low temperatures, $k_B T \ll \mu$, only a small region of energy near $\varepsilon = \mu$ contributes to the integral (6). In the case of $0 < \mu < \alpha$ and low temperatures, $k_B T \ll \mu$ and $k_B T \ll (\alpha - \mu)$, only the band corresponding to $n = 3$ contributes to the thermocurrent. It should be noted that in the case of an ordinary 2D electron gas with a parabolic energy spectrum, the thermoelectric current under these conditions is absent since the corresponding 2D density of states, ν_{2D}, is independent of the electron energy, and thus the currents due to particles and holes compensate each other, so the net current vanishes. In graphene, however, there is a nonzero thermoelectric ballistic current, which is related to the linear energy spectrum. This current is then equal to half of the total current in the graphene without Rashba coupling [see Eq. (8)]. Let us consider the case of $\mu > \alpha$. In this case there are contributions from both $n = 3$ and $n = 4$ bands. Assuming that $k_B T \ll (\mu - \alpha)$ we find

$$j \simeq \frac{e\pi k_B^2 T\,\Delta T}{15}\sum_n \frac{\partial}{\partial \varepsilon}\left[\nu_n(\varepsilon)\, v_n(\varepsilon)\right]\Big|_{\varepsilon=\mu}. \tag{7}$$

Since the energy dispersion in each band is parabolic near the edge, the 2D density of states is the step function $\nu_4(\varepsilon) \sim \theta(\varepsilon - \alpha)$, whereas the electron velocity $v_4(\varepsilon) \sim (\varepsilon - \alpha)^{1/2}$. Correspondingly, $\frac{\partial}{\partial \varepsilon}\left[\nu_n(\varepsilon)\, v_n(\varepsilon)\right]|_{\varepsilon=\mu} \sim (\mu - \alpha)^{-1/2}$, which means that the thermocurrent increases when we decrease μ. This growth stops at $(\mu - \alpha) \simeq k_B T$. In other words, there is a maximum in the dependence of the thermocurrent on μ. When $\mu \gg \alpha$, the influence of Rashba coupling disappears and the current becomes equal to that in a graphene with zero Rashba coupling, where there is a linear dependence of the density of states on the energy, $\nu(\varepsilon) = \varepsilon/\pi\hbar^2 v_F^2$ and $v(\epsilon) = v_F$. Then, assuming that $k_B T \ll \mu$, we find, for graphene in the ballistic regime,

$$j = \frac{e k_B^2 T\,\Delta T}{15\hbar^2 v_F}. \tag{8}$$

To compare the results for ballistic and diffusive junctions, we note that Eq. (4) also gives the thermoelectric current in the diffusive regime if we take $\Delta T = L\nabla T$ and substitute L by the mean free path ℓ, as it should be to match the ballistic and

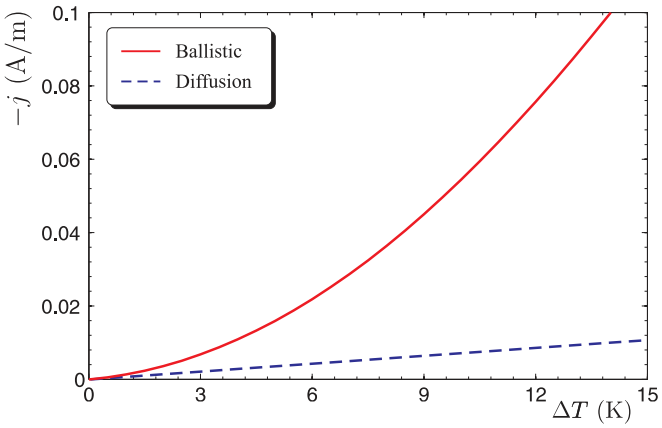

FIG. 3. (Color online) Comparison of the thermoelectrically induced current in the ballistic and diffusive transport regimes, calculated for $\mu = 5$ meV, $T = 1$ K, and $\alpha = 8$ meV. The electric current in the diffusive regime is proportional to the temperature difference ΔT.

diffusive results. Thus, if we keep $\nabla T = \text{const}$ and reduce ℓ, i.e., if we go to the diffusive regime by increasing the density of impurities, $\ell < L$, we decrease the current. The difference in the thermoelectric currents for ballistic versus diffusive transport regimes is shown in Fig. 3. For the case of diffusive transport we take $\ell = 100$ nm. While in the diffusive regime the thermocurrent increases linearly with the temperature difference ΔT, its increase with ΔT in the ballistic limit is faster and nonlinear.

One can also calculate the thermopower, or equivalently the thermally induced voltage U between the reservoirs under the condition of zero charge current, $j = 0$. To determine the voltage U, one can use Eq. (4) with the distribution functions corresponding to different electrochemical potentials, $\mu_1 \neq \mu_2$, as in Eq. (3). Then the voltage U can be determined from the condition that the thermally induced current is fully compensated by the field-induced current. The thermoelectric voltage is then given as $U = (\mu_1 - \mu_2)/e$. Results of the corresponding numerical calculation beyond the linear response regime are presented in Fig. 4. As follows from this figure, the thermoelectric voltage depends on the temperature difference in a nonlinear way, similarly as the thermocurrent. In turn, the dependence on the Rashba parameter is nonmonotonous and, also, resembles the corresponding dependence of the charge current.

B. Heat current

Employing the same method as that applied above in the calculation of the thermoelectric charge current, one can also calculate the heat current associated with transfer of electrons between the two reservoirs. The corresponding formula for the heat flux from the left reservoir (of temperature T_1) to the right one (of temperature T_2) can be written in the form

$$J_Q = \frac{1}{2}\sum_n \sum_{\mathbf{k}}{}' \langle \mathbf{k}n|\{(H_{\mathbf{k}} - \mu), \hat{v}_x\}|\mathbf{k}n\rangle \times [f_1^>(\varepsilon_{\mathbf{k}n}) - f_2^<(\varepsilon_{\mathbf{k}n})], \quad (9)$$

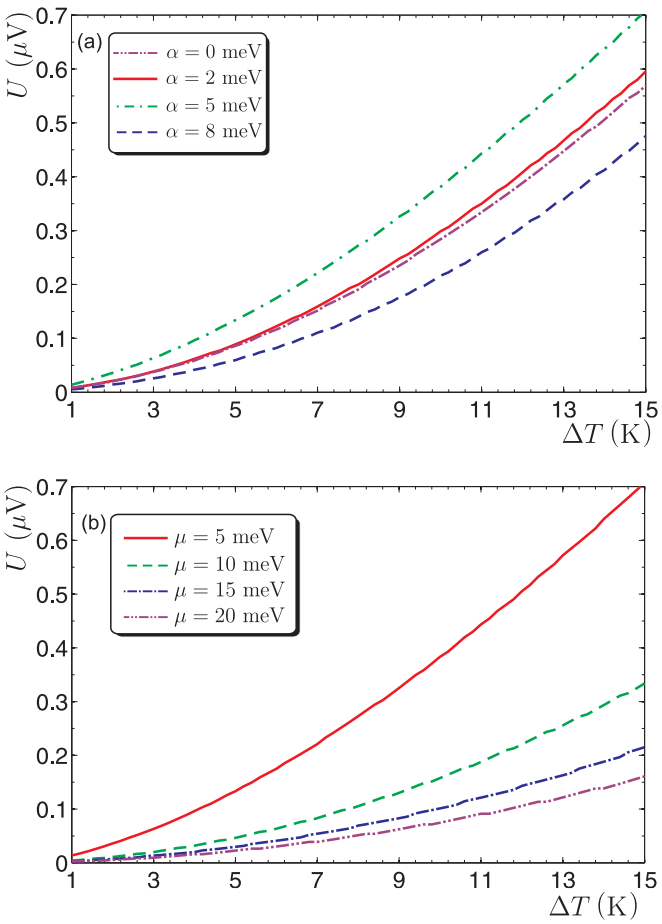

FIG. 4. (Color online) Thermoelectric voltage as a function of ΔT, calculated for $T = 1$ K and (a) $\mu = 5$ meV and indicated values of the Rashba parameter α or (b) $\alpha = 5$ meV and different values of the chemical potential μ.

where $\{\hat{A}, \hat{B}\}$ for any two operators $\hat{A}$ and $\hat{B}$ is defined as $\{\hat{A}, \hat{B}\} = \hat{A}\hat{B} + \hat{B}\hat{A}$.

The dependence of the heat current J_Q on the temperature difference ΔT is presented in Fig. 5(a) for different values of the Rashba parameter α. Similarly, as in the case of the charge current, the heat current increases nonlinearly with ΔT and, also, depends nonmonotonously on the Rashba parameter α [compare Figs. 2(a) and 5(a)].

Figure 5(b), in turn, shows the dependence of the heat current J_Q on the chemical potential μ. As follows from this figure, the dependence on μ is linear at large values of μ, $\mu \gg \alpha, kT_1, kT_2$, contrary to the behavior of the charge current, which saturates at large values of μ [see Fig. 2(b)]. This difference appears because the contribution to the heat current from a transferred electron depends on its energy, $\varepsilon \sim \mu$, while the corresponding contribution to the charge current is independent of this energy. As in the case of the charge current, the heat current for small values of α varies with μ similarly as in graphene with zero Rashba coupling [compare the curves for $\alpha = 0$ and $\alpha = 2$ meV in Fig. 5(b)]. However, when $\alpha - \mu > kT_1, kT_2$, the second conduction sub-band (corresponding to $n = 4$) does not contribute to the heat current. Surprisingly, the heat current is then higher than

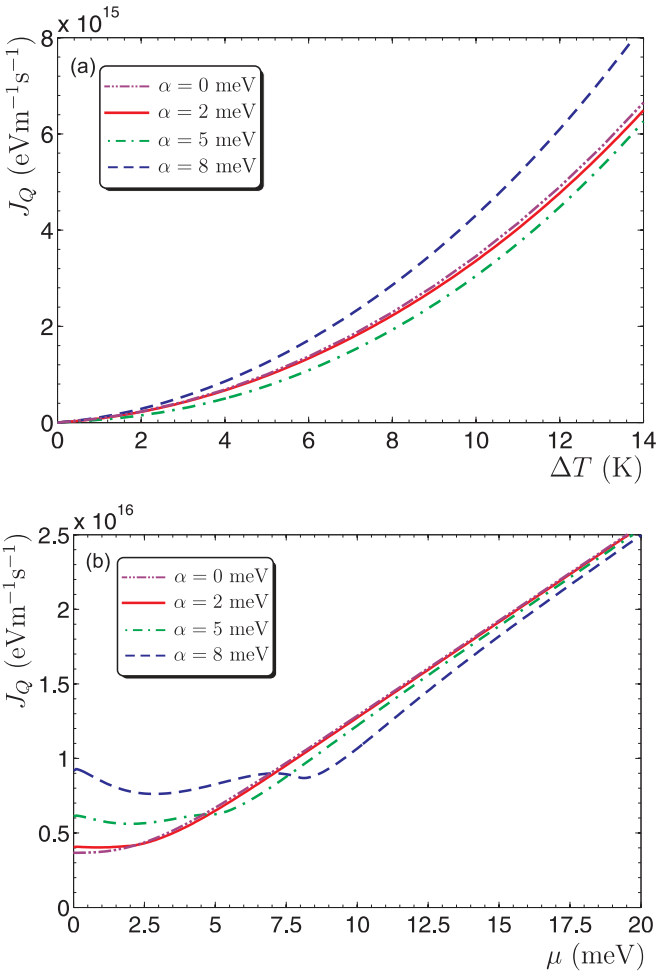

FIG. 5. (Color online) Heat current transmitted by electrons for $T = 1$ K and indicated values of the Rashba parameter α, calculated as a function of ΔT for $\mu = 5$ meV (a) and as a function of μ for $\Delta T = 14$ K (b).

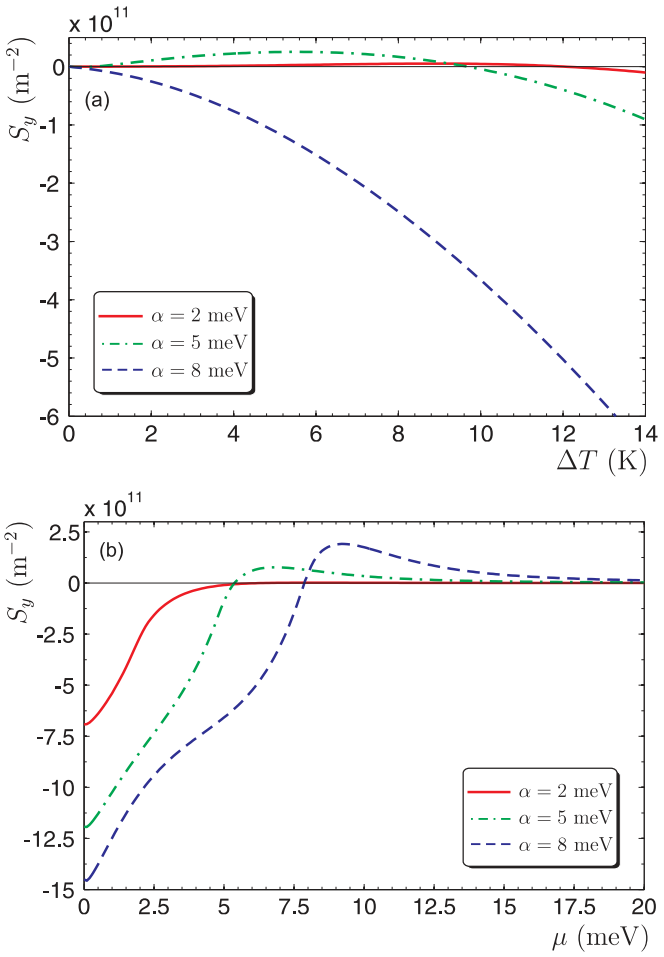

FIG. 6. (Color online) Thermoelectrically induced spin polarization for indicated values of the Rashba parameter and $T = 1$ K, calculated as a function of ΔT for $\mu = 5$ meV (a) and as a function of μ for $\Delta T = 14$ K (b).

that for $\alpha = 0$, contrary to the charge current, which is then lower [compare Figs. 5(b) and 2(b)]. This is an interplay effect of the increased density of states at the band edges due to the Rashba coupling and of the fact that the charge currents due to electrons and holes have opposite signs, while the corresponding heat currents then have the same sign. The heat current only weakly depends on μ for $\mu < \alpha$ and then increases with μ when $\mu > \alpha$, approaching the curve describing the heat current in a graphene with no Rashba interaction.

IV. THERMALLY INDUCED SPIN POLARIZATION AND SPIN CURRENT

As in the preceding section, we assume equal chemical potentials in the two electronic reservoirs, $\mu_1 = \mu_2 = \mu$. Below we calculate the spin polarization of electrons in graphene and the spin current, both induced by a temperature difference ΔT.

A. Spin polarization

It is already well known that spin-orbit interaction in the presence of either an electric field or a temperature gradient can induce spin polarization of conduction electrons. This effect has been studied theoretically for the usual 2D electron gas with a parabolic energy spectrum and Rashba spin-orbit coupling [45–47], as well as in graphene [44]. In the ballistic junction considered in this paper, the spin density (measured in units of $\hbar/2$) can be calculated using the formula

$$S_\alpha = \sum_n \sum_{\mathbf{k}}{}' \langle \mathbf{k}n|\sigma_\alpha|\mathbf{k}n\rangle [f_1^>(\varepsilon_{\mathbf{k}n}) - f_2^<(\varepsilon_{\mathbf{k}n})]. \quad (10)$$

The corresponding numerical results are presented in Fig. 6, where the thermally induced spin polarization along the axis y, S_y, is shown as a function of ΔT [Fig. 6(a)] and as a function of μ [Fig. 6(b)]. The induced spin polarization is in the graphene plane and is normal to the temperature gradient, similarly as in the diffuse transport regime in a 2D electron gas [47]. Obviously, the spin polarization vanishes for $\alpha = 0$. If $\alpha \lesssim kT_1, kT_2$, the spin polarization S_y is negative and approaches 0 when $\mu \gg \alpha$. In turn, when $\alpha \gg kT_1, kT_2$, then the spin polarization is also negative for

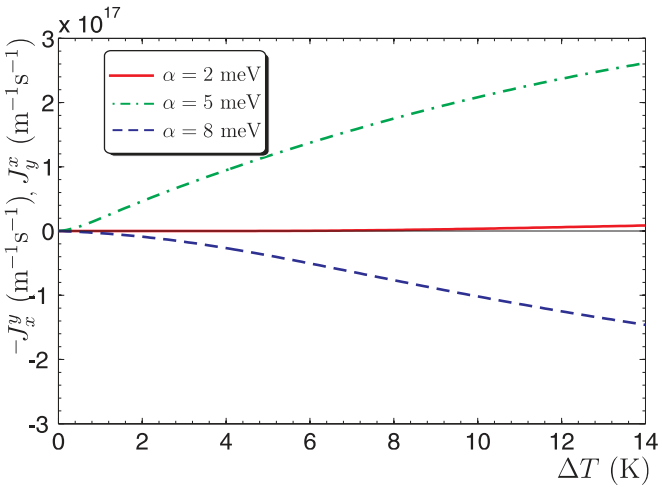

FIG. 7. (Color online) Thermally induced spin currents J_x^y and J_y^x for different values of α, calculated as a function of ΔT for $\mu = 5$ meV and $T = 1$ K.

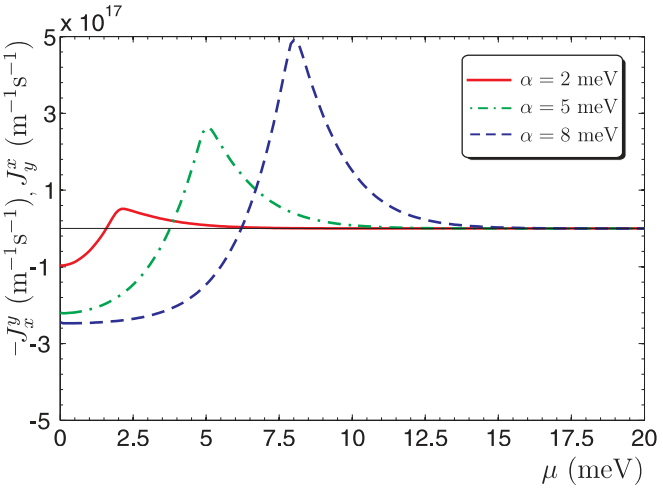

FIG. 8. (Color online) Thermally induced spin currents J_x^y and J_y^x for different values of α, calculated as a function of μ for $\Delta T = 14$ K and $T = 1$ K.

$\mu < \alpha$, but it changes sign around $\mu \approx \alpha$, reaching a weak maximum, and then tends to 0 for $\mu \gg \alpha$, where the dispersion relations become linear as in graphene with vanishing Rashba coupling. The physical mechanism of the spin polarization in graphene with Rashba spin-orbit coupling is also similar to the mechanism of spin polarization in a 2D electron gas. Indeed, there is a nonzero spin polarization of an electron in the eigenstate $|\mathbf{k}n\rangle$, which is perpendicular to the wave vector $\mathbf{k}$. The magnitude of this spin polarization is small for $k \ll \alpha/\hbar v_F$ and is equal to its maximum value equal to $\hbar/2$ for $k \gg \alpha/\hbar v_F$ [48]. A nonzero spin polarization S_y appears due to the imbalance of the distribution of electrons with $k_x > 0$ and $k_x < 0$ [44]. In turn, the origin of the maximum is similar to that in the case of the charge current, as discussed above.

B. Spin currents

The temperature difference between the electron reservoirs can also generate a spin current J_x^y flowing parallel to the temperature gradient as well as a spin current J_y^x flowing perpendicularly to the gradient. Here the upper index indicated the spin component associated with the spin current, while the lower index indicated the orientation of the spin current flow. Both components of the spin current can be calculated using the same method as in the case of the charge current. The relevant formula now takes the form

$$J_i^\alpha = \frac{1}{2}\sum_n \sum_{\mathbf{k}}{}' \langle \mathbf{k}n|\{\sigma_\alpha, \hat{v}_i\}|\mathbf{k}n\rangle [f_1^>(\varepsilon_{\mathbf{k}n}) - f_2^<(\varepsilon_{\mathbf{k}n})]. \quad (11)$$

Taking into account the contributions from a particular quantum state to both spin current components and integrating over all incidence angles, one can show that $J_x^y = -J_y^x$. Indeed this was also proven numerically, by calculating the currents J_x^y and J_y^x from Eq. (11).

The numerical results for both J_x^y and J_y^x calculated as a function of the temperature difference ΔT are presented in Fig. 7, and those as a function of the chemical potential μ in Fig. 8. The mechanism of a nonzero component J_x^y is related to the spin polarization of electrons due to the temperature gradient and Rashba spin-orbit interaction, as calculated and discussed above. These spin-polarized electrons are transferred between the two electron reservoirs, giving rise to the spin current J_x^y. In turn, the other spin current component, J_y^x, corresponds to the thermally induced spin Hall effect, also called the spin Nernst effect [41]. This effect consists in a spin current generation by a temperature gradient. The induced current flows then perpendicularly to the temperature gradient.

V. SUMMARY

We have analyzed thermoelectric and thermospin effects in a ballistic graphene ribbon attached to two electronic reservoirs of different temperatures. The graphene ribbon was assumed to be deposited on a substrate that generated a strong spin-orbit coupling of the Rashba type. We have calculated not only the thermally induced charge current between the two reservoirs and the associated thermoelectric voltage, but also the thermally induced spin polarization and spin current. Numerical results on the charge current show that the current in the ballistic regime is significantly higher than in the diffusive one.

The spin current, in turn, is shown to have two components. One of them is related to the thermally induced spin polarization of electrons transferred from one reservoir to the other, while the other one reveals the spin Nernst effect, i.e., the thermally induced spin Hall effect. We have also calculated the heat transferred by ballistic electrons from the reservoir of higher temperature to the reservoir of lower temperature.

In our calculation we used various values of the parameter α. As is known, the magnitude of the Rashba spin-orbit interaction depends on the substrate. In some cases it can be very strong, for example, $\alpha = 225$ meV for graphene on Ni(111) [49], $\alpha = 100$ meV for graphene on gold [50], and $\alpha = 50$ meV for graphene on Ir(111) [51].

ACKNOWLEDGMENTS

This work was supported by the National Science Center in Poland as Research Project Nos. DEC-2012/06/M/ST3/00042 (M.I.) and DEC-2012/04/A/ST3/00372 (V.K.D. and J.B.). The work of M.I. is also supported by the Project Nos. POIG.01.04.00-18-101/12 and UDA-RPPK.01.03.00-18-025/13-00.

[1] A. H. Castro Neto, F. Guinea, N. M. R. Peres, K. S. Novoselov, and A. K. Geim, Rev. Mod. Phys. **81**, 109 (2009).
[2] E. B. Sonin, Phys. Rev. B **79**, 195438 (2009).
[3] M. I. Katsnelson, K. S. Novoselov, and A. K. Geim, Nature Phys. **2**, 620 (2006).
[4] G. H. Lee, S. Kim, S. H. Jhi, and H. J. Lee, Nature Commun. **6**, 6181 (2015).
[5] M. F. Borunda, H. Hennig, and E. J. Heller, Phys. Rev. B **88**, 125415 (2013).
[6] A. L. Grushina, D. K. Ki, and A. F. Morpurgo, Appl. Phys. Lett. **102**, 223102 (2013).
[7] N. T. T. Nguyen, D. Q. To, and V. L. Nguyen, J. Phys. Condens. Matter **26**, 015301 (2014).
[8] M. Titov and C. W. J. Beenakker, Phys. Rev. B **74**, 041401(R) (2006).
[9] A. Yamakage, K. I. Imura, J. Cayssol, and Y. Kuramoto, Phys. Rev. B **83**, 125401 (2011).
[10] M. Rataj and J. Barnaś, Phys. Status Solidi: Rapid Res. Lett. **7**, 997 (2013).
[11] A. A. Balandin, S. Ghosh, W. Bao, I. Calizo, D. Teweldebrahn, F. Miao, and C. Lau, Nano Lett. **8**, 902 (2008).
[12] M. Wierzbowska, A. Dominiak, and G. Pizzi, 2D Mater. **1**, 035002 (2014).
[13] M. Wierzbowska and A. Dominiak, Carbon **80**, 255 (2014).
[14] M. Wierzbicki, R. Swirkowicz, and J. Barnaś, Phys. Rev. B **88**, 235434 (2013).
[15] M. S. Foster and I. L. Aleiner, Phys. Rev. B **79**, 085415 (2009).
[16] P. Wei, W. Bao, Y. Pu, C. N. Lau, and J. Shi, Phys. Rev. Lett. **102**, 166808 (2009).
[17] X. Z. Yan, Y. Romiah, and C. S. Ting, Phys. Rev. B **80**, 165423 (2009).
[18] Y. M. Zuev, W. Chang, and P. Kim, Phys. Rev. Lett. **102**, 096807 (2009).
[19] V. Ugarte, V. Aji, and C. M. Varma, Phys. Rev. B **84**, 165429 (2011).
[20] D. Wang and J. Shi, Phys. Rev. B **83**, 113403 (2011).
[21] S. G. Sharapov and A. A. Varlamov, Phys. Rev. B **86**, 035430 (2012).
[22] M. I. Alomar and D. Sánchez, Phys. Rev. B **89**, 115422 (2014).
[23] J. H. Seol, I. Jo, A. L. Moore, L. Lindsay, Z. H. Aitken, M. T. Pettes, X. Li, Z. Yao, R. Huang, D. Broido, N. Mingo, R. S. Ruoff, and L. Shi, Science **328**, 213 (2010).
[24] D. Dragoman and M. Dragoman, Appl. Phys. Lett. **91**, 203116 (2007).
[25] T. Stauber, N. M. R. Peres, and F. Guinea, Phys. Rev. B **76**, 205423 (2007).
[26] M. Inglot, A. Dyrdal, V. K. Dugaev, and J. Barnaś, Phys. Rev. B **91**, 115410 (2015).
[27] Y. Xu, Z. Li, and W. Duan, Small **10**, 2182 (2014).
[28] X. H. Zheng, G. R. Zhang, Z. Zeng, V. M. Garcia-Suarez, and C. J. Lambert, Phys. Rev. B **80**, 075413 (2009).
[29] Y.-T. Zhang, Q. M. Li, Y. C. Li, Y. Y. Zhang, and F. Zhai, J. Phys.: Condens. Matter **22**, 315304 (2010).
[30] Z. Aksamija and I. Knezevic, Phys. Rev. B **90**, 035419 (2014).
[31] H. Sevincli and G. Cuniberti, Phys. Rev. B **81**, 113401 (2010).
[32] W. Huang, J. S. Wang, and G. Liang, Phys. Rev. B **84**, 045410 (2011).
[33] P. H. Chang and B. K. Nikolić, Phys. Rev. B **86**, 041406(R) (2012).
[34] L. Liang, E. Cruz-Silva, E. C. Girao, and V. Meunier, Phys. Rev. B **86**, 115438 (2012).
[35] W. Chen and A. A. Clerk, Phys. Rev. B **86**, 125443 (2012).
[36] L. Lindsay, Wu Li, J. Carrete, N. Mingo, D. A. Broido, and T. L. Reinecke, Phys. Rev. B **89**, 155426 (2014).
[37] H. Jaffrès, Physics **7**, 123 (2014).
[38] M. Oltscher, M. Ciorga, M. Utz, D. Schuh, D. Bougeard, and D. Weiss, Phys. Rev. Lett. **113**, 236602 (2014).
[39] A. S. Mayorov, R. V. Gorbachev, S. V. Morozov, L. Britnell, R. Jalil, L. A. Ponomarenko, P. Blake, K. S. Novoselov, K. Watanabe, T. Taniguchi, and A. K. Geim, Nano Lett. **11**, 2396 (2011).
[40] J. Baringhaus, M. Ruan, F. Edler, A. Tejeda, M. Sicot, A. Taleb-Ibrahimi, A. P. Li, Z. Jiang, E. H. Conrad, C. Berger, C. Tegenkamp, and W. A. de Heer, Nature **506**, 349 (2014).
[41] V. P. Gusynin, S. G. Sharapov, and A. A. Varlamov, Phys. Rev. B **90**, 155107 (2014).
[42] N. A. Sinitsyn, J. E. Hill, Hongki Min, J.o Sinova, and A. H. MacDonald, Phys. Rev. Lett. **97**, 106804 (2006).
[43] J. Balakrishnan, G. K. W. Koon, A. Avsar, Y. Ho, J. H. Lee, M. Jaiswal, S.-J. Baeck, J.-H. Ahn, A. Ferreira, M. A. Cazalilla, A. H. Castro Neto, and B. Ozyilmaz, Nature Commun. **5**, 4748 (2014).
[44] A. Dyrdal, J. Barnaś, and V. K. Dugaev, Phys. Rev. B **89**, 075422 (2014).
[45] V. M. Edelstein, Solid State Commun. **73**, 233 (1990).
[46] A. G. Aronov and Y. B. Lynda-Geller, JETP Lett. **50**, 431 (1989).
[47] A. Dyrdal, M. Inglot, V. K. Dugaev, and J. Barnaś, Phys. Rev. B **87**, 245309 (2013).
[48] E. I. Rashba, Phys. Rev. B **79**, 161409 (2009).
[49] Yu. S. Dedkov, M. Fonin, U. Rüdiger, and C. Laubschat, Phys. Rev. Lett. **100**, 107602 (2008).
[50] D. Marchenko, A. Varykhalov, M. R. Scholz, G. Bihlmayer, E. I. Rashba, A. Rybkin, A. M. Shikin, and O. Rader, Nature Commun. **3**, 1232 (2012).
[51] D. Marchenko, J. Sánchez-Barriga, M. R. Scholz, O. Rader, and A. Varykhalov, Phys. Rev. B **87**, 115426 (2013).